photonics

MDPI

Article

Enhanced Signal of Sum Sideband via Parametric Interactions in a Mechanical PT-Symmetric System

Hui Zheng, Zihan Du and Aixi Chen *

Zhejiang Key Laboratory of Quantum State Control and Optical Field Manipulation, Department of Physics, Zhejiang Sci-Tech University, Hangzhou 310018, China; 2023210104040@mails.zstu.edu.cn (H.Z.); 2024210104009@mails.zstu.edu.cn (Z.D.)

* Correspondence: aixichen@zstu.edu.cn

Abstract

We investigate a double-probe-field-driven cavity optomechanical system with a degenerate optical parametric amplifier (OPA). When the system is in a mechanical PT-symmetric case, we study the generation mechanism of the sum sideband and how to enhance the generation efficiency of the sum sideband by controlling parametric interactions. Our model consists of two directly coupled PT-symmetric mechanical resonators, which are coupled to a Fabry–Pérot cavity equipped with an optical parametric amplifier. Research indicates that in a PT-symmetric mechanical resonator, there exist special exceptional points (EPs). Near EPs, the generation efficiency of the sum sideband is significantly enhanced. Notably, the introduction of an OPA can remarkably boost the efficiency of sum sideband generation (SSG) and establish a new sideband matching condition for the upper sum sideband. We conduct a detailed analysis of the dependence of SSG on system parameters, such as mechanical coupling strength, OPA nonlinear gain, OPA pump light field phase, and probe field frequency detuning. The research reveals that even with a weak driving field, a significantly enhanced efficiency of SSG can be achieved by adjusting the OPA gain coefficient and phase. This research offers new insights into enhancing or regulating light propagation in nonlinear optomechanical devices and holds potential for applications in high-precision measurement and optical communication.

Keywords: PT-symmetric; optical parametric amplifier; sum sideband

1. Introduction

Cavity optomechanics [1] is an interdisciplinary subject that fuses quantum physics, optics, and mechanics, spotlighting the coupling mechanism between optical fields and macro mechanical oscillators [2]. The theoretical origin of this realm can be blame to the intersection of quantum optics and Classic mechanics, and it has now become an important platform for studying the quantum-to-classical transition [3] phenomenon. In recent years, driven by the rapid development of micro-nano technology [4], cavity optomechanics has received extensive follow and achieved remarkable progress. In the quantum cavity optomechanics framework, the interaction [1] between the quantity of photons in the cavity and the quantum state of mechanical vibration affords researchers a way to explore cutting-edge problems such as quantum measurement [5], quantum entanglement [6], and quantum information processing. In addition, this realm also provides unique technical means for developing new types of sensors, achieving precision measurements, and constructing quantum computing systems [7].

Check for updates

Received: 24 November 2025
Revised: 18 January 2026
Accepted: 7 February 2026
Published: 13 February 2026

Copyright: © 2026 by the authors. Licensee MDPI, Basel, Switzerland. This article is an open access article distributed under the terms and conditions of the Creative Commons Attribution (CC BY) license.

Optomechanically induced transparency (OMIT) refers to the phenomenon in optomechanical systems where a strong driving field induces a tunable transparency window for a weak probe [8]. Its mechanism is a mechanical analogy to electromagnetically induced transparency, achieving destructive quantum interference in optical modes through optomechanical interactions, resulting in the suppression of resonant absorption [9], and has been verified in experiments [10,11]. In recent years, research related to OMIT has received extensive attentions [9,11–26]. For example, optomechanical induced transparency is produced in excited atomic medium [27]. Noteworthy is that in an optomechanical system driven by two weak probe fields, while retaining the nonlinear effects caused by optomechanical interaction, the generation of sum and difference sidebands can be achieved [24–26,28], which is different from the traditional optomechanical model driven by a single probe field [9,11–23]. Early studies have explored the mechanism of SSG in universal optomechanical systems under the parameter conditions of optomechanically induced transparency [7]. Another work has achieved sum sideband generation of Laguerre-Gaussian light beams through orbital angular momentum exchange [29]. Since the sum sideband efficiency is of great significance for high-precision measurement and optical communication research, its enhancement methods have become a recent hot spot. Studies have shown that under the action of dual radiation pressure [30] or the ingestion of two-level atoms [31], the sum sideband efficiency in the composite optomechanical system can be enhanced.

In recent years, research on non-Hermitian PT symmetry has drawn extensive attention in the field of optics. This symmetry can be achieved by introducing balanced gain and loss into optical systems [32,33]. Souvik Mondal et al. [34] utilized a continuous-wave pump laser to modulate the oscillation amplitude in a PT symmetry structure, thereby enabling control of the sidebands. Flexible regulation of OMIT can also be achieved in a second-order coupled PT symmetry optomechanical system [35]. By applying PT symmetry to coupled optomechanical systems [36], one can investigate the sum sideband efficiency of the system. Research indicates that by adjusting the system to be near the gain-loss EPs [36], the sum sideband efficiency can be significantly enhanced. The combination of optomechanics and non-Hermitian PT-symmetric systems offers many new perspectives for studying the interaction between light and matter.

An optical parametric amplifier (OPA) is widely used due to its strong nonlinearity. Its intrinsic noise is lower than that of traditional amplifiers based on stimulated emission, so when using a stable pump, it is often used as a key device to achieve low-noise signal amplification in optomechanical systems. It is widely applied in multi-body entanglement [37], mechanical oscillator cooling [38,39], and optomechanically induced transparency [40]. In recent years, the applications of OPA in optomechanical systems and sidebands have also been gradually explored. The presence of OPA can significantly enhance the efficiency of the SSG even with low power input [41]. This phenomenon also occurs in the quadratic coupling optomechanical system [42]. Moreover, research shows that the amplitude of the second-order sideband can be modulated and amplified by OPA, which is driven by distinct pump frequencies [43].

This study will investigate the influence of OPA on SSG in a non-Hermitian PT-symmetric system co-driven by a strong control field and two weak probe fields. The model is inspired by the scheme of a PT-symmetric mechanical resonator proposed by Bao Wang et al. [44]. An OPA is added to the cavity mode of this model to investigate the generation of the sideband. The results demonstrate that with the introduction of the OPA, the SSG efficiency can be significantly enhanced even at lower input powers compared to general optomechanical systems [28]. This enhancement is most pronounced when the system is near the critical points (EPs) separating the PT- symmetry phase from the broken phase. More intriguingly, a new matching criterion for the upper sum sideband generation (USSG)

emerges due to the addition of OPA. Moreover, as the gain coefficient of OPA increases, both the windows and peaks of the USSG and lower sum sideband generation (LSSG) grow. Subsequently, the influence of the pump field's phase on the sum sideband was also discussed. To better understand the new matching conditions for the upper sum sideband, we also discuss the functional relationship of the USSG efficiency with respect to δ_1 and δ_2.

The structure of this paper is organized as follows. In Section 2, the model to be studied is described and analyzed. The composition of the total Hamiltonian is explained, and the derivation processes of the motion equations of system operators and the efficiency of the upper and lower sidebands are presented. In the Section 3, the exceptional point EPs is first identified, and the PT-symmetric phase and the PT-broken phase are explained through the combination of numbers and shapes. Subsequently, different experimental parameters are numerically varied, and the results are analyzed and discussed using images. In Section 4, the results of the numerical analysis are summarized.

2. Theoretical Model and Formulations

Our theoretical model is shown in Figure 1, where the hybrid optomechanical system consists of a Fabry–Pérot cavity, which consists of two directly coupled PT-symmetric mechanical resonators (MR), and it also contains an OPA. In order to increase the coupling of the cavity field with the mechanical oscillator, a control field with a frequency of ω_c excites the cavity with a resonant frequency of ω_0. In addition, two weak probe fields with frequencies of ω_i ($i = 1, 2$) propagate inside the cavity and couple with the cavity field. The mechanical resonator b_1 is coupled with the cavity field by the optical radiation pressure. Moreover, the MR b_1 with a loss rate γ_1 is coupled to the MR b_2 with a gain rate γ_2 via the coupling parameter J. $\varepsilon_c = \sqrt{P_c/\hbar\omega_c}$ denotes the amplitude of the control field, while $\varepsilon_i = \sqrt{P_i/\hbar\omega_i}$ ($i = 1, 2$) represent the amplitude of the probe fields. Here, P_c and P_i ($i = 1, 2$), respectively, represent the pump power of the control field and the probe field's power.

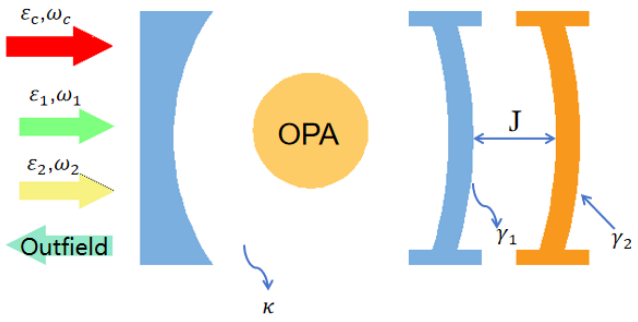

Figure 1. Schematic diagram of the PT-symmetric system containing an OPA. The system is driven by a strong control field with frequency ω_c, along with two relatively weak probe lasers with frequencies ω_1 and ω_2, respectively.

Now, in the rotating coordinate system at the frequency ω_c of the control field, the complete Hamiltonian formulation of the system can be written as:

$$\begin{aligned} H =& \hbar\Delta a^{\dagger}a + \hbar\omega_m(b_1^{\dagger}b_1 + b_2^{\dagger}b_2) - \hbar g a^{\dagger}a(b_1^{\dagger} + b_1) - \hbar J(b_1^{\dagger}b_2 + b_1 b_2^{\dagger}) \\ &+ i\hbar G\left(e^{i\theta}a^{\dagger 2}e^{-2i\omega_c t} - e^{-i\theta}a^2 e^{2i\omega_c t}\right) + i\hbar\sqrt{\kappa/2}\varepsilon_c(a^{\dagger} + a) \\ &+ i\hbar\sqrt{\kappa/2}\left[(\varepsilon_1 a^{\dagger}e^{-i\delta_1 t} - \varepsilon_2 a^{\dagger}e^{-i\delta_2 t}) - \mathrm{H.C}\right], \end{aligned} \tag{1}$$

where the detuning $\Delta = \omega_0 - \omega_c$ and it is the detuning between the control field and cavity field. $\delta_i = \omega_i - \omega_c$ ($i = 1, 2$) stands for the detuning between the control and the weak field. g denotes the optomechanical coupling strength, θ and G represent the phase of the field

driving the OPA and the nonlinear gain of the OPA, respectively, which can be adjusted through pump driving. ω_m is the intrinsic frequency of the MR and κ is the total cavity loss rate.

Under the condition where the cavity field is driven by the strong control field, we focus on the average response of the system to the probe field, and the quantum and thermal noise terms are ignored. The losses of the cavity field and the resonator are added phenomenologically, so the simplified Heisenberg-Langevin equations of motion for the operators operating on the system can be expressed as

$$\begin{aligned}
\dot{a} &= \left[-i\Delta - \frac{\kappa}{2} + ig(b_1^\dagger + b_1)\right]a + 2Ge^{i\theta}a^\dagger + \sqrt{\kappa/2}(\varepsilon_c + \varepsilon_1 e^{-i\delta_1 t} + \varepsilon_2 e^{-i\delta_2 t}),\\
\dot{b}_1 &= \left(-i\omega_m - \frac{\gamma_1}{2}\right)b_1 + iJb_2 + iga^\dagger a,\\
\dot{b}_2 &= \left(-i\omega_m + \frac{\gamma_2}{2}\right)b_2 + iJb_1.
\end{aligned} \tag{2}$$

Comparingwith the intensity of the probe field, the intensity of the control field is sufficiently large, so we may use the linear approximation method to handle the system's dynamic equations with $a = \bar{a} + \delta a$, $b_i = \bar{b}_i + \delta b_i$, ($i$ = 1, 2). Substituting them into Equation (2), firstly, we can obtain the steady-state values of the system

$$\begin{aligned}
\bar{a} &= \frac{\sqrt{\kappa/2}\varepsilon_c\left(2Ge^{i\theta} + \frac{\kappa}{2} + 2iG\sin\theta - i\bar{\Delta}\right)}{\frac{\kappa^2}{4} + \bar{\Delta}^2 - 4G^2},\\
\bar{b}_1 &= \frac{ig|\bar{a}|^2\left(i\omega_m - \frac{\gamma_2}{2}\right)}{\left(i\omega_m + \frac{\gamma_1}{2}\right)\left(i\omega_m - \frac{\gamma_2}{2}\right) + J^2},\\
\bar{b}_2 &= \frac{iJ\bar{b}_1}{i\omega_m - \frac{\gamma_2}{2}}.
\end{aligned} \tag{3}$$

where $\bar{\Delta} = \Delta - g(\bar{b}_1^* + \bar{b}_1)$ is the effective detuning of the cavity containing radiation pressure. According to the steady-state value, we can find that the photon number inside the cavity is primarily influenced by the optomechanical coupling effect and the introduction of OPA. Furthermore, the expression of $\bar{b}_1$ includes parameter γ_2, i.e., the photon number of MR1 is affected by the gain of MR2. Due to the mutual coupling between various subsystems, the mutual influence between these physical quantities is caused, which means that when considering the impact of the PT-symmetric MR on the entire cavity field, the output spectrum of the probe field will be manipulated. Here we will discuss the signal of the sum sidebands. Next, we consider the dynamic equations of the fluctuation caused by the probe field. For the perturbation terms, the quantum Langevin equation is obtained as:

$$\begin{aligned}
\delta\dot{a} &= \left(-i\bar{\Delta} - \frac{\kappa}{2}\right)\delta a + ig[\bar{a}(\delta b_1^* + \delta b_1) + \delta a(\delta b_1^* + \delta b_1)] + 2Ge^{i\theta}\delta a^* + \sqrt{\kappa/2}(\varepsilon_1 e^{-i\delta_1 t} + \varepsilon_2 e^{-i\delta_2 t}),\\
\delta\dot{b}_1 &= \left(-i\omega_m - \frac{\gamma_1}{2}\right)\delta b_1 + iJ\delta b_2 + ig(\bar{a}^*\delta a + \bar{a}\delta a^* + \delta a\delta a^*),\\
\delta\dot{b}_2 &= \left(-i\omega_m + \frac{\gamma_2}{2}\right)\delta b_2 + iJ\delta b_1.
\end{aligned} \tag{4}$$

In order to study the nonlinear effects of optomechanics, we need to retain some second-order small quantities of optomechanical coupling in Equation (4). For example, the second-order small quantities $\delta a(\delta b_1^* + \delta b_1)$ and $\delta a\delta a^*$ are very key to the SSG. Here, the SSG in the mechanical PT-symmetric system is similar to that of high-order sideband under the mechanism of optomechanically induced transparency. Generally, in an effort

to analyze the sum sideband and second-order sideband, the perturbation terms may be expanded under the following assumptions.

$$\begin{aligned}
\delta a &= A_1^+ e^{-i\delta_1 t} + A_1^- e^{i\delta_1 t} + A_2^+ e^{-i\delta_2 t} + A_2^- e^{i\delta_2 t} + A_s^+ e^{-i\Omega t} + A_s^- e^{i\Omega t} + \cdots, \\
\delta b_1 &= B_1^+ e^{-i\delta_1 t} + B_1^- e^{i\delta_1 t} + B_2^+ e^{-i\delta_2 t} + B_2^- e^{i\delta_2 t} + B_s^+ e^{-i\Omega t} + B_s^- e^{i\Omega t} + \cdots, \\
\delta b_2 &= C_1^+ e^{-i\delta_1 t} + C_1^- e^{i\delta_1 t} + C_2^+ e^{-i\delta_2 t} + C_2^- e^{i\delta_2 t} + C_s^+ e^{-i\Omega t} + C_s^- e^{i\Omega t} + \cdots.
\end{aligned} \tag{5}$$

here, $\Omega = \delta_1 + \delta_2$. The frequency components at $\pm\Omega$ are called sum sideband, and $A_s^{\pm}, B_s^{\pm}, C_s^{\pm}$ are the coefficients of these components. In our research work, we are only interested in the first-order sideband and sum sideband processes. In other words, we disregard the higher-order sidebands in the above equations. By substituting Equation (5) into Equation (4), 18 algebraic equations for the coefficients are obtained. According to the properties of the sideband, the 18 equations are divided into two parts. The first part corresponds to the coefficient equation of the first-order sideband, which describes the process of the probe field with a frequency of $\omega_1(\omega_2)$.

$$\begin{aligned}
-i\delta_1 A_1^+ &= \left(-i\overline{\Delta} - \frac{\kappa}{2}\right) A_1^+ + ig\bar{a}(B_1^{-*} + B_1^+) + 2Ge^{i\theta} A_1^{-*} + \sqrt{\kappa/2}\varepsilon_1, \\
-i\delta_1 B_1^+ &= \left(-i\omega_m - \frac{r_1}{2}\right) B_1^+ + ig(\bar{a}^* A_1^+ + \bar{a} A_1^{-*}) + iJC_1^+, \\
-i\delta_1 C_1^+ &= \left(-i\omega_m + \frac{r_2}{2}\right) C_1^+ + iJB_1^+, \\
i\delta_1 A_1^- &= \left(-i\overline{\Delta} - \frac{\kappa}{2}\right) A_1^- + ig\bar{a}(B_1^{+*} + B_1^-) + 2Ge^{i\theta} A_1^{+*}, \\
i\delta_1 B_1^- &= \left(-i\omega_m - \frac{r_1}{2}\right) B_1^- + ig(\bar{a}^* A_1^- + \bar{a} A_1^{+*}) + iJC_1^-, \\
i\delta_1 C_1^- &= \left(-i\omega_m + \frac{r_2}{2}\right) C_1^- + iJB_1^-, \\
-i\delta_2 A_2^+ &= \left(-i\overline{\Delta} - \frac{\kappa}{2}\right) A_2^+ + ig\bar{a}(B_2^{-*} + B_2^+) + 2Ge^{i\theta} A_2^{-*} + \sqrt{\kappa/2}\varepsilon_2, \\
-i\delta_2 B_2^+ &= \left(-i\omega_m - \frac{r_1}{2}\right) B_2^+ + ig(\bar{a}^* A_2^+ + \bar{a} A_2^{-*}) + iJC_2^+, \\
-i\delta_2 C_2^+ &= \left(-i\omega_m + \frac{r_2}{2}\right) C_2^+ + iJB_2^+, \\
i\delta_2 A_2^- &= \left(-i\overline{\Delta} - \frac{\kappa}{2}\right) A_2^- + ig\bar{a}(B_2^{+*} + B_2^-) + 2Ge^{i\theta} A_2^{+*}, \\
i\delta_2 B_2^- &= \left(-i\omega_m - \frac{r_1}{2}\right) B_2^- + ig(\bar{a}^* A_2^- + \bar{a} A_2^{+*}) + iJC_2^-, \\
i\delta_2 C_2^- &= \left(-i\omega_m + \frac{r_2}{2}\right) C_2^- + iJB_2^-.
\end{aligned} \tag{6}$$

where the nonlinear terms in the optomechanical dynamics are neglected, and the values of the coefficients of the sum sideband are related to the solutions of these equations. The second part describes the process of SSG, in which the nonlinear terms of optomechanical dynamics are also retained:

$$\begin{aligned}
-i\Omega A_s^+ &= \left(-i\bar{\Delta} - \frac{\kappa}{2}\right) A_s^+ + ig\left[\bar{a}\left(B_1^{-^*} + B_1^+\right) + A_1^+ B_2^{-^*} + A_1^+ B_2^+ + A_2^+ B_1^{-^*} + A_2^+ B_1^+\right] + 2Ge^{i\theta} A_s^{-^*}, \\
-i\Omega B_s^+ &= \left(-i\omega_m - \frac{\gamma_1}{2}\right) B_s^+ + ig\left(\bar{a}^* A_s^+ + \bar{a} A_s^{-^*} + A_1^+ A_2^{-^*} + A_2^+ A_1^{-^*}\right) + iJC_s^+, \\
-i\Omega C_s^+ &= \left(-i\omega_m + \frac{\gamma_2}{2}\right) C_s^+ + iJB_s^+, \\
i\Omega A_s^- &= \left(-i\bar{\Delta} - \frac{\kappa}{2}\right) A_s^- + ig\left[\bar{a}\left(B_s^{+^*} + B_s^-\right) + A_1^- B_2^{+^*} + A_1^- B_2^- + A_2^- B_1^{+^*} + A_2^- B_1^-\right] + 2Ge^{i\theta} A_s^{+^*}, \\
i\Omega B_s^- &= \left(-i\omega_m - \frac{\gamma_1}{2}\right) B_s^- + ig\left(\bar{a}^* A_s^- + \bar{a} A_s^{+^*} + A_1^- A_2^{+^*} + A_2^- A_1^{+^*}\right) + iJC_s^-, \\
i\Omega C_s^- &= \left(-i\omega_m + \frac{\gamma_2}{2}\right) C_s^- + iJB_s^-.
\end{aligned} \tag{7}$$

We have previously stated that Equation (6) describes the linear process of the probe field with frequencies $\omega_1(\omega_2)$. This process has been explored in previous studies and utilized to investigate double phonons optomechanically induced transparency [35]. The solutions of Equations (6) and (7) are (where $i = 1, 2$)

$$\begin{aligned} A_i^+ &= \frac{\sqrt{\kappa/2}\varepsilon_i L'_-(\delta_i)^* L_+(\delta_i)\beta_-(\delta_i)^*}{\beta_+(\delta_i)\beta_-(\delta_i)^* - \varphi_-(\delta_i)\varphi_+(\delta_i)^*}, \quad A_i^- = \frac{\varphi_+(\delta_i)}{\beta_-(\delta_i)} A_1^{+*}, \\ B_i^- &= \frac{-ig\left(\bar{a}^* A_i^- + \bar{a} A_i^{+^*}\right) E'_-(\delta_i)}{L'_-(\delta_i)}, \quad B_i^+ = \frac{ig\left(\bar{a}^* A_i^+ + \bar{a} A_i^{-*}\right) E_+(\delta_i)}{L_+(\delta_i)}, \\ A_s^- &= \frac{\varphi_+(\Omega)\psi_-(\Omega)^* + \psi_+(\Omega)\beta_+(\Omega)^*}{\beta_-(\Omega)\beta_+(\Omega)^* - \varphi_+(\Omega)\varphi_-(\Omega)^*}, \quad A_s^+ = \frac{\varphi_-(\Omega) A_s^{-^*} + \psi_-(\Omega)}{\beta_+(\Omega)}. \end{aligned} \tag{8}$$

where

$$\begin{aligned} &F_\pm(x) = i\Delta + \frac{\kappa}{2} \mp i\delta_i - ig(\overline{b_1}^* + \overline{b_1}), \quad D_\pm(x) = \frac{\gamma_1}{2} \pm i\omega_m - ix, \quad D'_\pm(x) = -\frac{\gamma_1}{2} \pm i\omega_m - ix, \\ &E_\pm(x) = -\frac{\gamma_2}{2} \pm i\omega_m - ix, \quad E'_\pm(x) = \frac{\gamma_2}{2} \pm i\omega_m - ix, \quad L_\pm(x) = D_\pm(x)E_\pm(x) + J^2, \\ &L'_\pm(x) = D'_\pm(x)E'_\pm(x) + J^2, \quad \alpha(x) = L_+(x)E'_-(x)^* + E_+(x)L'_-(x)^*, \\ &\beta_+(x) = F_+(x)L_+(x)L'_-(x)^* + g^2|\bar{a}|^2\alpha(x), \quad \beta_-(x) = F_-(x)L_+(x)^*L'_-(x) - g^2|\bar{a}|^2\alpha(x)^*, \\ &\varphi_-(x) = -g^2\bar{a}^2\alpha(x) + 2Ge^{i\theta}L_+(x)L'_-(x)^*, \quad \varphi_+(x) = g^2\bar{a}^2\alpha'(x) + 2Ge^{i\theta}L_+(x)^*L'_-(x), \\ &\phi_1^* = A_1^- B_2^{+*} + A_1^- B_2^- + A_2^- B_1^{+*} + A_2^- B_1^-, \quad \phi_2 = A_1^+ B_2^{-*} + A_1^+ B_2^+ + A_2^+ B_1^{-*} + A_2^+ B_1^+, \\ &\phi_3 = A_1^+ A_2^{-*} + A_2^+ A_1^{-*}, \quad \psi_+(\Omega) = \bar{a}g^2\phi_3^*\alpha(\Omega)^* + ig\phi_1^* L'_-(\Omega)L_+(\Omega)^*, \\ &\psi_-(\Omega) = -\bar{a}g^2\phi_3\alpha(\Omega) + ig\phi_2 L_+(\Omega)L'_-(\Omega)^* \end{aligned}$$

The values of x in the expression are $\delta_1, \delta_2, \Omega$. It can be seen that the sum sideband amplitudes of $A_s^\pm$ show an intense correlation on the nonlinear gain G and the OPA phase θ. By applying the standard input-output relation, namely $a_{out} = a_{in} - \sqrt{\kappa/2}a$, the output field of the system in the reference frame rotating at ω_c can be obtained as follows:

$$\begin{aligned} a_{out} = (\varepsilon_c - \sqrt{\kappa/2}\bar{a}) + (\varepsilon_1 - \sqrt{\kappa/2}A_1^+)e^{-i\delta_1 t} - \sqrt{\kappa/2}A_1^- e^{i\delta_1 t} + (\varepsilon_2 - \sqrt{\kappa/2}A_2^+)e^{-i\delta_2 t} \\ - \sqrt{\kappa/2}A_2^- e^{i\delta_2 t} - \sqrt{\kappa/2}A_s^+ e^{-i\Omega t} - \sqrt{\kappa/2}A_s^- e^{i\Omega t}. \end{aligned} \tag{9}$$

$(\varepsilon_c - \sqrt{\kappa/2}\bar{a}), (\varepsilon_1 - \sqrt{\kappa/2}A_1^+)e^{-i\delta_1 t}$ and $(\varepsilon_2 - \sqrt{\kappa/2}A_2^+)e^{-i\delta_2 t}$ describe the output fields with frequencies ω_c and $\omega_1(\omega_2)$. Meanwhile, $-\sqrt{\kappa/2}A_s^+ e^{-i\Omega t}$ and $-\sqrt{\kappa/2}A_s^- e^{i\Omega t}$ describe the outputs with frequencies $\omega_c \pm \Omega$, corresponding to the upper sideband and lower sideband, respectively.

Here, only the sum sidebands are considered. The efficiencies of the upper and lower sum sidebands are, respectively, defined as $\eta_s^+ = \left|-\sqrt{\kappa/2}A_s^+/\varepsilon_1\right|$ and $\eta_s^- = \left|-\sqrt{\kappa/2}A_s^-/\varepsilon_1\right|$, which represent the amplitude ratios of the sum sideband to the first probe field; these efficiencies are dimensionless. Previous studies have shown that when δ_1 and δ_2 reach specific values, the efficiency of SSG shows a peak structure. The specific values of $\delta_1(\delta_2)$corresponding to these peaks are referred to as the matching condition.

3. Results and Discussion

In this section, we study the transmission characteristics of the two probe fields in the mechanical PT-symmetric optomechanical configuration and discuss how the nonlinear gain of OPA and phase affect the sum sideband efficiency based on this configuration.

3.1. Mechanical PT-Symmetric Configuration

The condition for mechanical PT symmetry is obtained by adiabatically eliminating the optical mode. Here, the effective optomechanical coupling $G_1 = ga$ and the intrinsic decay rates γ_1,γ_2 are assumed to be smaller than κ, i.e., $\{G_1, \gamma_1, \gamma_2 \ll \kappa\}$. Therefore, the effective non-Hermitian Hamiltonian can be expressed as

$$H_{eff} = (\omega_m - i\gamma_1/2)b_1^\dagger b_1 + (\omega_m + i\gamma_2/2)b_2^\dagger b_2 - J(b_1^\dagger b_2 + b_1 b_2^\dagger). \tag{10}$$

The matrix representation of Equation (10) is as follows:

$$H_{eff} = \begin{pmatrix} b_1^\dagger & b_2^\dagger \end{pmatrix} \begin{pmatrix} \omega_m - i\gamma_1/2 & -J \\ -J & \omega_m + i\gamma_2/2 \end{pmatrix} \begin{pmatrix} b_1 \\ b_2 \end{pmatrix}. \tag{11}$$

Among them, the characteristic frequencies $b_1 \pm b_2$ of the corresponding mechanical modes are calculated as

$$\omega_\pm = \omega_m - i\frac{(\gamma_1 - \gamma_2)}{4} \pm \sqrt{J^2 - \left(\frac{\gamma_1 + \gamma_2}{4}\right)^2}. \tag{12}$$

Figure 2, respectively, presents the real and imaginary parts of the eigenfrequencies calculated using Equation (11). When the coupling rate exceeds $\frac{\gamma_1+\gamma_2}{4}$, i.e., $J > \frac{\gamma_1+\gamma_2}{4}$, the PT-symmetric phase is observed. At this point, $Re(\omega_\pm)$ splits around ω_m, while their imaginary parts $Im(\omega_\pm)$ remain the same. If the coupling rate is below $\frac{\gamma_1+\gamma_2}{4}$, namely $J < \frac{\gamma_1+\gamma_2}{4}$, the system enters the PT-broken phase, where the two modes degenerate, with one mode experiencing gain while the other undergoes loss, and their imaginary parts point in opposite directions. This is clearly illustrated in Figure 2. When the mechanical oscillator coupling strength J equals the effective loss rate $\frac{\gamma_1+\gamma_2}{4}$, it leads to a critical point known as Eps.

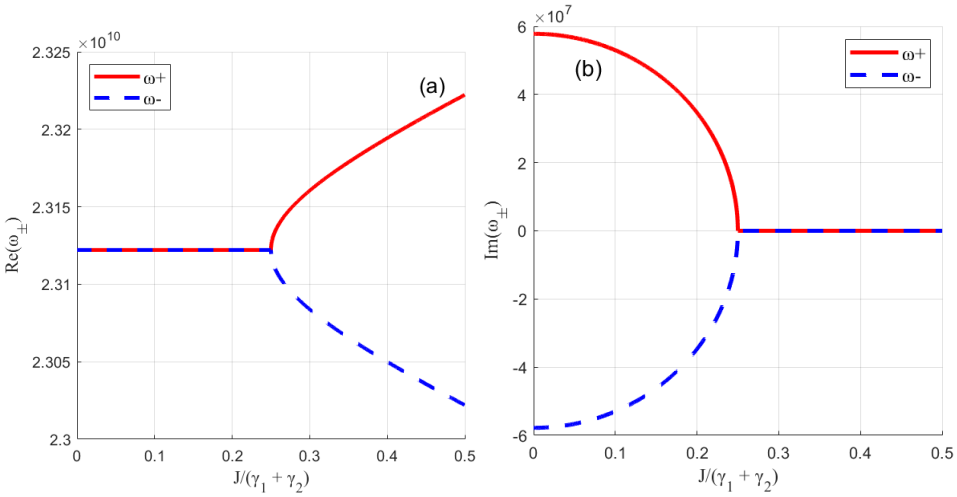

Figure 2. (**a**) The real part of the eigenvalues of PT-symmetric MR as functions of J; (**b**) The imaginary part of the eigenvalues of PT-symmetric MR as functions of J.

3.2. Adjustable Sum Sideband Controlled by System Parameters

In this section, we will use numerical methods to explore the efficiency of SSG in a PT-symmetric cavity optomechanical system with an OPA. Notably, the nonlinearity of the OPA can significantly alter the characteristics of the cavity field and enhance the sideband efficiency.

First, we will investigate how the PT-symmetric property impacts the SSG efficiency by varying the mechanical coupling parameter J. Next, with the mechanical coupling

parameter set at $J = \frac{\gamma_1+\gamma_2}{4}$, at this time, we will analyze the substantial influence of the OPA on SSG by adjusting the nonlinear gain coefficient G and the field phase θ. Finally, we will discuss the effect of the detuning frequency $\delta_i (i = 1, 2)$ between the control field and the first and second probe fields on the efficiency of SSG in the cavity optomechanical system with the OPA. The primary parameters employed here are derived from recent research [45,46], $\lambda = 1573$ nm, $g = 2\pi$ MHz, $\omega_m/2\pi = 3.68$ GHz, $\kappa = 0.1\omega_m$, $\gamma_1 = \gamma_2 = 0.5 \times 10^{-2}\,\omega_m$.

The coupling strength J of PT-symmetric mechanical resonators exerts a significant influence on the SSG. As illustrated in Figure 3, the efficiency of the SSG transitions from weak to strong as the value of J increases. Particularly near the EPs, the SSG efficiency exhibits a remarkable enhancement. In Figure 3a, a radiation peak and a transparency window emerge in the vicinity of the EPs. From a physical perspective, near the EPs, the gain of one mechanical resonator continuously compensates for the loss of the other mechanical resonators, and the lossy mechanical oscillator induces the dynamic accumulation of acoustic energy due to magnetic field localization [47]. This enhances the optomechanical nonlinear effect, which significantly modulates the up-conversion process field during this mechanism, thereby improving the generation efficiency of the anti-Stokes field. As the mechanical coupling strength J increases, the sum sideband splits into two radiation peaks. Concurrently, as illustrated in Figure 3c, the transparency window splits into two absorption peaks. Notably, when compared to the conventional optomechanical system with a single mechanical resonator (blue solid line in Figure 3c), the USSG efficiency exhibits significant amplification near the EPs. Similarly, as shown in Figure 3b, the LSSG radiation peak undergoes substantial enhancement near the EPs and splits into four distinct radiation peaks with increasing mechanical coupling strength J. The LSSG efficiency is also significantly enhanced compared to the conventional optomechanical system (blue solid line in Figure 3d), as depicted in Figure 3d.

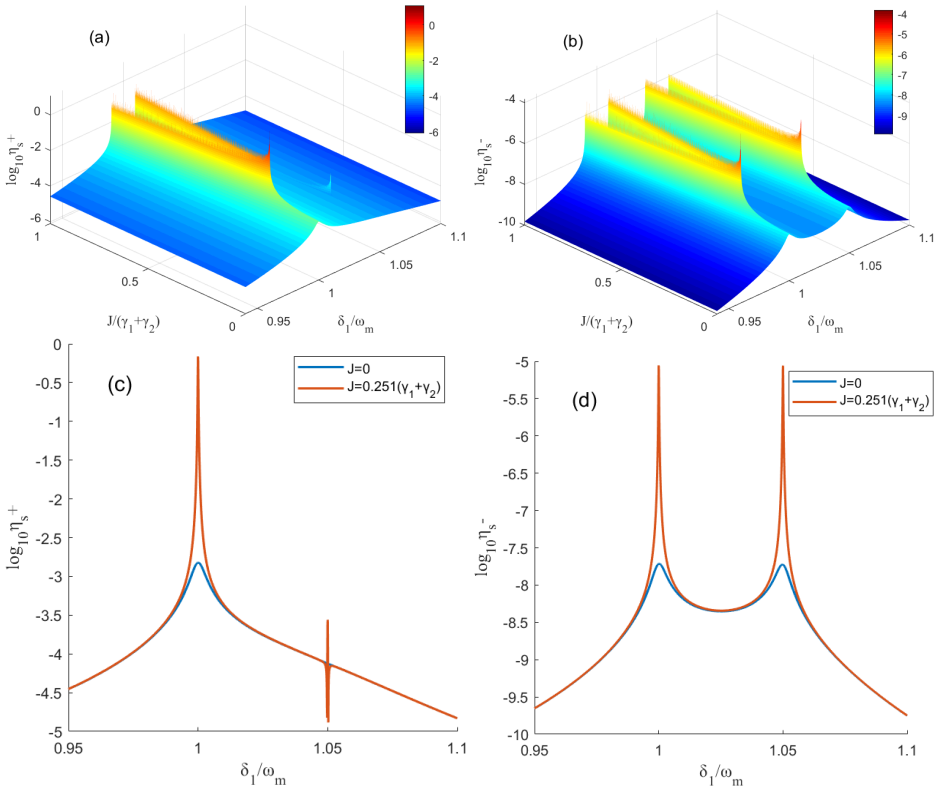

Figure 3. (**a**) The efficiency of USSG and (**b**) LSSG (expressed in logarithmic form) varies with the mechanical coupling strength J and detuning frequency δ_1. (**c**) The efficiency of USSG and (**d**) LSSG varies with the detuning frequency δ_1. We use $G = 0$, $P_c = 1$ μW, $\delta_2 = -0.05\,\omega_m$, $P_1 = P_2 = 0.05$ μW.

To demonstrate the significant influence of OPA on the generation of the upper and lower sum sidebands, Figure 4 below shows how the generation efficiency (in logarithmic form) of these sidebands varies with the frequency of the first probe field δ_1. As shown in Figure 4, OPA significantly enhances the efficiency of the USSG. To simplify the analysis, we assume that the phase θ of the field driving the OPA is zero. As shown in Figure 4a, without OPA, when $G = 0$, the logarithmic efficiency $\log_{10}\eta_s^+$ of the upper sideband has only one peak within the parameter range $0.95\omega_m < \delta_1 < 1.1\omega_m$. Additionally, without OPA, when the detuning between the control field and cavity field $\Delta = \omega_m$, the upper sum sideband generates an absorption peak at $\delta_1 = 1.05\omega_m$. The physical explanation for this phenomenon is that when the resonance condition $\Delta = \omega_m$ is met, the excitation of the mechanical oscillator causes destructive interference in the excitation path of the intracavity probe field, which in turn leads to the formation of a transparency window for the intracavity probe field. Since the choices of δ_1 and δ_2 satisfy the relationship $\delta_1 + \delta_2 = \omega_m$, which is close to the resonance condition $\Delta = \omega_m$ of the cavity, a new peak appears at $\delta_1 = 1.05\omega_m$ when $G \neq 0$. Therefore, the matching conditions for $\log_{10}\eta_s^+$ can be adjusted to $\delta_1 = \omega_m$ and $\delta_1 + \delta_2 = \omega_m$, which differs from the scenario without OPA, where a new matching condition $\delta_1 + \delta_2 = \omega_m$ is introduced. Moreover, when OPA is present, and $G = 0.4\kappa$, the efficiency of USSG at $\delta_1 = 1.05\omega_m$ is over 100 times higher than that in the absence of OPA. As shown in Figure 4b, the peak structure of LSSG remains unchanged regardless of whether G exists or not. It can also be observed from Figure 4b that when OPA is present and $G = 0.4\kappa$, the efficiency of LSSG at $\delta_1 = \omega_m$ is about 1%. In the absence of OPA, due to the weak optomechanical nonlinearity, the efficiency of LSSG, $\log_{10}\eta_s^-$ is extremely low. The efficiency of LSSG is approximately 1×10^{-4}%. Obviously, when OPA is added, the efficiency of LSSG can be improved by several orders of magnitude. In other words, the presence of G has a significant impact on the efficiency of SSG.

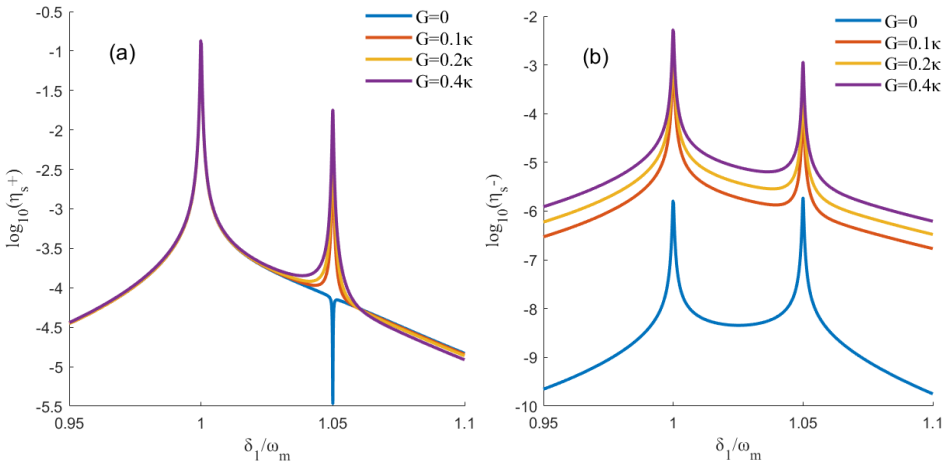

Figure 4. Shows the efficiency (in logarithmic form) of (**a**) USSG and (**b**) LSSG, which varies with the frequency of the first probe field δ_1. The experimental parameters are set as follows: power density P_c = 1 μW, $P_1 = P_2 = 0.05$ μW, $\delta_2 = -0.05\,\omega_m$, $\theta = 0$, $J = \frac{\gamma_1+\gamma_2}{4}$, and different values of G.

Next, we will explore how the phase θ affects the sum sideband generation efficiency. Figure 5a,b, respectively, illustrate how the efficiencies of the upper and lower sidebands vary with the detuning δ_1 and phase θ of the OPA. As shown in the Figure 5, the efficiency distribution exhibits distinct interference fringe characteristics, which directly verifies that sideband generation is a coherent nonlinear process whose efficiency strongly depends on the total phase-matching condition. Due to the periodicity of the phase factor $e^{i\theta}$, the system efficiency exhibits a 2π periodicity with respect to θ, and reaches a peak at a specific value of θ, which directly reflects the system's phase interference behavior. This indicates

that even if the frequency condition is satisfied, coherent constructive interference will be disrupted, and the efficiency will drop sharply if the phase condition is not matched. More importantly, the efficiency distributions in Figure 5a,b may exhibit the characteristic of mutually "peaking out of phase" along the θ axis, which reveals that the phase θ acts as a nonlinear "routing switch" and can dynamically selectively direct the pump energy to the upper sideband or lower sideband channel. It is evident that the efficiency of the sum sideband is highly sensitive to changes in the OPA phase. Specifically, when δ_1 ranges from $1.05\omega_m$–$1.15\omega_m$, the phase θ has a more significant impact on the sum sideband efficiency.

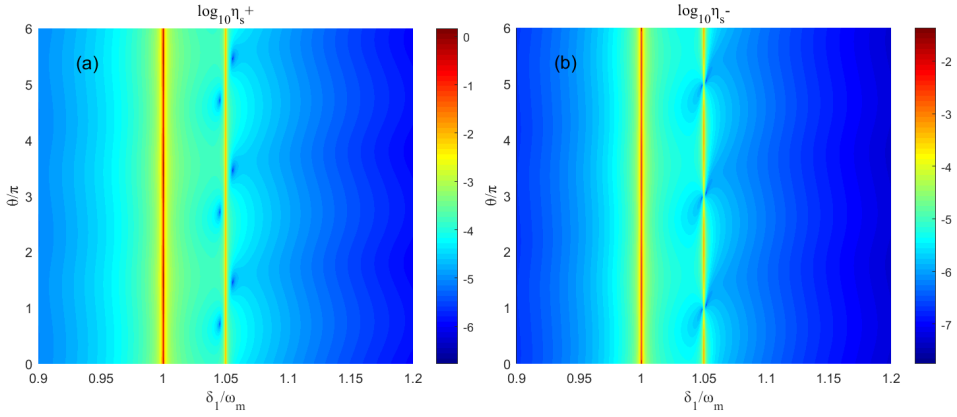

Figure 5. The calculated values of (**a**) $\log_{10}\eta_s^+$ and (**b**) $\log_{10}\eta_s^-$ change with δ_1 and θ, where $G = 0.3\kappa$. The other parameters are the same as those in Figure 4.

Figure 6a displays the calculated efficiency of upper and lower sideband generation (in logarithmic form) as a function of δ_1 and δ_2, revealing a distinct peak structure at specific δ_1 and δ_2 values. This behavior is associated with particular phase-matching conditions for SSG. As shown in Figure 6c, in the absence of an OPA, near EPs, the USSG efficiency of the PT symmetry mechanical resonator reaches its maximum when the conditions $\delta_1 = \pm\omega_m$, $\delta_2 = \pm\omega_m$, and $\delta_1 + \delta_2 = \omega_m$ are satisfied. This introduces an additional matching condition $\delta_1 + \delta_2 = \omega_m$ compared to conventional optomechanical systems [28]. With the OPA activated, as illustrated in Figure 6a, the matching conditions for maximum USSG efficiency near EPs in the PT symmetry mechanical resonator become $\delta_1 = \pm\omega_m$, $\delta_2 = \pm\omega_m$, and $\delta_1 + \delta_2 = \pm\omega_m$. The influence of the OPA identifies a new matching condition $\delta_1 + \delta_2 = -\omega_m$, which once again results in a peak efficiency for the upper sideband. Notably, the improvement of efficiency is more pronounced when $\delta_1 + \delta_2 = \omega_m$ compared to $\delta_1 + \delta_2 = -\omega_m$. This difference arises because the former condition, $\delta_1 + \delta_2 = \omega_m$, lies closer to the cavity resonance condition $\Delta = \omega_m$. For the LSSG in Figure 6b, compared to Figure 6d, it is found that the LSSG not only retains the same matching condition but also exhibits a remarkably high generation efficiency.

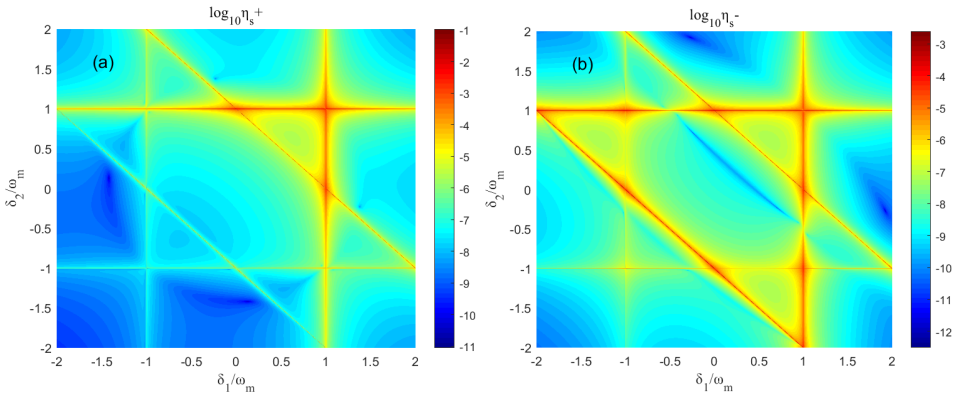

Figure 6. *Cont.*

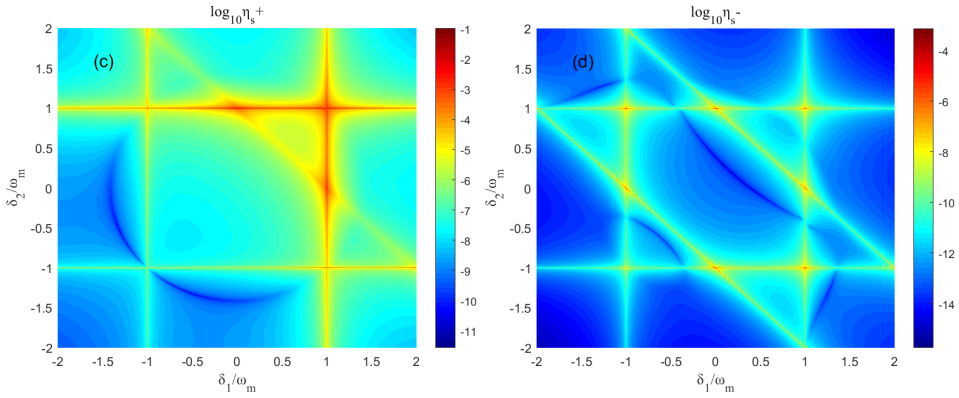

Figure 6. Showsthe efficiency (in logarithmic form) of USSG and LSSG with respect to δ_1 and δ_2. Where, in figures (**a**,**b**) we use $G = 0.3\kappa$, and (**c**,**d**) we use $G = 0$, other parameters are the same as those in Figure 4.

4. Conclusions

In summary, we summarized a numerical analysis of a mechanical PT-symmetric system under two probe fields, focusing on the roles of OPA pairs and sidebands. Through numerical calculations and analysis, a special point EPs was found in the PT-symmetric mechanical resonator. Near EPs, the efficiency of SSG significantly improved, and will generate a new upper sum sideband matching condition. As the coupling strength J between the PT-symmetric mechanical resonators increased, the PT-symmetric phase was observed, during which the upper sum sideband split near the detuning frequency ω_m. The presence of OPA can change the matching conditions of the USSG, giving rise to a new sideband matching condition, attributed to its influence on the system's nonlinear dynamics. This converts the destructive interference, which originally occurred at the detuning frequency $1.05\omega_m$ for the USSG due to the properties of EPs, into a new peak. Additionally, by adjusting the gain coefficient and phase of the OPA, the efficiency of the LSSG can be enhanced by several orders of magnitude. The study provides valuable insights into light propagation in nonlinear optomechanical systems, with direct relevance for the fields of high-precision measurement and optical communications.

Author Contributions: Conceptualization, formal analysis, methodology, resources, writing—review and editing, H.Z. and A.C.; data curation, software, visualization, writing—original draft, H.Z.; investigation, Z.D.; validation, H.Z. and Z.D.; funding acquisition, project administration, A.C. All authors have read and agreed to the published version of the manuscript.

Funding: This work was supported by the National Natural Science Foundation of China (No. 12575031).

Data Availability Statement: Data generated during the current study will be made available upon reasonable request.

Conflicts of Interest: The authors declare no conflicts of interest.

References

1. Aspelmeyer, M.; Kippenberg, T.J.; Marquardt, F. Cavity optomechanics. *Rev. Mod. Phys.* **2014**, *86*, 1391–1452. [CrossRef]
2. Martin, I.; Shnirman, A.; Tian, L.; Zoller, P. Ground-state cooling of mechanical resonators. *Phys. Rev. B* **2004**, *69*, 125339. [CrossRef]
3. Zang, H.; Tan, H.; Li, G. Research progress on nonclassical mechanical states in cavity optomechanics. *Sci. Sin. Phys. Mech. Astron.* **2023**, *53*, 290008. [CrossRef]
4. Ziaie, B.; Baldi, A.; Atashbar, M. Introduction to micro/nanofabrication. In *Springer Handbook of Nanotechnology*; Springer: Berlin/Heidelberg, Germany, 2007; pp. 197–238.

5. Buffoni, L.; Solfanelli, A.; Verrucchi, P.; Cuccoli, A.; Campisi, M. Quantum measurement cooling. *Phys. Rev. Lett.* **2019**, *122*, 070603. [CrossRef]
6. Liu, Y.Y.; Zhang, Z.M.; Liu, J.H.; Wang, J.D.; Yu, Y.F. Nonreciprocal coupling induced entanglement enhancement in a double-cavity optomechanical system. *Chin. Phys. B* **2022**, *31*, 094203. [CrossRef]
7. Chen, X.; Liu, X.W.; Zhang, K.Y.; Yuan, C.H.; Zhang, W.P. Quantum measurement with cavity optomechanical systems. *Wuli Xuebao/Acta Phys. Sin.* **2015**, *64*, 164211. [CrossRef]
8. Xu, X.W.; Song, L.; Zheng, Q.; Wang, Z.; Li, Y. Optomechanically induced nonreciprocity in a three-mode optomechanical system. *Phys. Rev. A* **2018**, *98*, 063845. [CrossRef]
9. Agarwal, G.S.; Huang, S. Electromagnetically induced transparency in mechanical effects of light. *Phys. Rev. A—At. Mol. Opt. Phys.* **2010**, *81*, 041803. [CrossRef]
10. Safavi-Naeini, A.H.; Alegre, T.M.; Chan, J.; Eichenfield, M.; Winger, M.; Lin, Q.; Hill, J.T.; Chang, D.E.; Painter, O. Electromagnetically induced transparency and slow light with optomechanics. *Nature* **2011**, *472*, 69–73. [CrossRef]
11. Weis, S.; Rivière, R.; Deléglise, S.; Gavartin, E.; Arcizet, O.; Schliesser, A.; Kippenberg, T.J. Optomechanically induced transparency. *Science* **2010**, *330*, 1520–1523. [CrossRef]
12. Yan, X.B. Optomechanically induced transparency and gain. *Phys. Rev. A* **2020**, *101*, 043820. [CrossRef]
13. Wu, S.C.; Qin, L.G.; Jing, J.; Yang, G.H.; Wang, Z.Y. Triple optomechanical induced transparency in a two-cavity system. *Chin. Phys. B* **2016**, *25*, 054203. [CrossRef]
14. Xiao, R.j.; Pan, G.x.; Liu, Y. Tunable multicolor optomechanically induced transparency in multi-cavity optomechanical system. *Int. J. Theor. Phys.* **2020**, *59*, 3256–3267. [CrossRef]
15. Ma, P.C.; Zhang, J.Q.; Xiao, Y.; Feng, M.; Zhang, Z.M. Tunable double optomechanically induced transparency in an optomechanical system. *Phys. Rev. A* **2014**, *90*, 043825. [CrossRef]
16. Zhang, X.; Zhou, Y.; Guo, Y.; Yi, X. Optomechanically induced transparency in optomechanics with both linear and quadratic coupling. *Phys. Rev. A* **2018**, *98*, 053802. [CrossRef]
17. Huang, S.; Agarwal, G. Electromagnetically induced transparency from two-phonon processes in quadratically coupled membranes. *Phys. Rev. A—At. Mol. Opt. Phys.* **2011**, *83*, 023823. [CrossRef]
18. Zhang, X.; Guo, Y.; Pei, P.; Yi, X. Optomechanically induced absorption in parity-time-symmetric optomechanical systems. *Phys. Rev. A* **2017**, *95*, 063825. [CrossRef]
19. Pan, G.; Yu, G.; Xiao, R.; Zhai, C. Controlling double optomechanically induced transparency and slow/fast light in an electro-optomechanical system via an optical parametric amplifier. *Laser Phys.* **2023**, *33*, 105202. [CrossRef]
20. Gu, W.j.; Yi, Z. Double optomechanically induced transparency in coupled-resonator system. *Opt. Commun.* **2014**, *333*, 261–264. [CrossRef]
21. Zhan, X.G.; Si, L.G.; Zheng, A.S.; Yang, X. Tunable slow light in a quadratically coupled optomechanical system. *J. Phys. B At. Mol. Opt. Phys.* **2013**, *46*, 025501. [CrossRef]
22. Li, B.B.; Ou, L.; Lei, Y.; Liu, Y.C. Cavity optomechanical sensing. *Nanophotonics* **2021**, *10*, 2799–2832. [CrossRef]
23. Lai, D.G.; Wang, X.; Qin, W.; Hou, B.P.; Nori, F.; Liao, J.Q. Tunable optomechanically induced transparency by controlling the dark-mode effect. *Phys. Rev. A* **2020**, *102*, 023707. [CrossRef]
24. Xiong, H.; Fan, Y.W.; Yang, X.; Wu, Y. Radiation pressure induced difference-sideband generation beyond linearized description. *Appl. Phys. Lett.* **2016**, *109*. [CrossRef]
25. Smith, D.D.; Chang, H.; Fuller, K.A.; Rosenberger, A.; Boyd, R.W. Coupled-resonator-induced transparency. *Phys. Rev. A—At. Mol. Opt. Phys.* **2004**, *69*, 063804. [CrossRef]
26. Xiao, R.J.; Pan, G.X.; Xiu, X.M. Controlling multiple optomechanically induced transparency in the distant cavity-optomechanical system. *Chin. Phys. B* **2021**, *30*, 034209. [CrossRef]
27. Nie, W.; Chen, A.; Lan, Y. Optical-response properties in levitated optomechanical systems beyond the low-excitation limit. *Phys. Rev. A* **2016**, *93*, 023841. [CrossRef]
28. Xiong, H.; Si, L.G.; Lü, X.Y.; Wu, Y. Optomechanically induced sum sideband generation. *Opt. Express* **2016**, *24*, 5773–5783. [CrossRef]
29. Xiong, H.; Huang, Y.M.; Wu, Y. Laguerre-Gaussian optical sum-sideband generation via orbital angular momentum exchange. *Phys. Rev. A* **2021**, *103*, 043506. [CrossRef]
30. Liao, Q.; Ao, J.; Song, M.; Qiu, H. Generation and enhancement of the sum sideband under double radiation pressure. *Opt. Express* **2023**, *31*, 27508–27519. [CrossRef]
31. Liao, Q.; Tang, Z.; Ao, J. Sum sideband effect in hybrid optomechanical system with two-level atom ensemble. *Acta Phys. Sin.* **2025**, *74*, 084206. [CrossRef]
32. El-Ganainy, R.; Makris, K.G.; Khajavikhan, M.; Musslimani, Z.H.; Rotter, S.; Christodoulides, D.N. Non-Hermitian physics and PT symmetry. *Nat. Phys.* **2018**, *14*, 11–19. [CrossRef]

33. Özdemir, Ş.K.; Rotter, S.; Nori, F.; Yang, L. Parity–time symmetry and exceptional points in photonics. *Nat. Mater.* **2019**, *18*, 783–798. [CrossRef] [PubMed]
34. Mondal, S.; Debnath, K. Controllable optical-sideband generation and synchronization in a mechanical gain-loss optomechanical system. *Phys. Rev. A* **2023**, *108*, 023517. [CrossRef]
35. Lu, X.H.; Si, L.G.; Wang, B.; Wang, X.Y.; Wu, Y. Tunable optomechanically induced transparency in a gain-assisted optomechanical system. *J. Phys. B At. Mol. Opt. Phys.* **2019**, *52*, 085401. [CrossRef]
36. Lu, X.H.; Si, L.G.; Wang, X.Y.; Wu, Y. Exceptional points enhance sum sideband generation in a mechanical PT-symmetric system. *Opt. Express* **2021**, *29*, 4875–4886. [CrossRef]
37. Xuereb, A.; Barbieri, M.; Paternostro, M. Multipartite optomechanical entanglement from competing nonlinearities. *Phys. Rev. A—At. Mol. Opt. Phys.* **2012**, *86*, 013809. [CrossRef]
38. Pan, Q.; Lv, W.; Deng, L.; Huang, S.; Chen, A. Cooling a Rotating Mirror Coupled to a Single Laguerre–Gaussian Cavity Mode Using Parametric Interactions. *Nanomaterials* **2022**, *12*, 3701. [CrossRef]
39. Huang, S.; Agarwal, G. Enhancement of cavity cooling of a micromechanical mirror using parametric interactions. *Phys. Rev. A—At. Mol. Opt. Phys.* **2009**, *79*, 013821. [CrossRef]
40. Yu, G.; Pan, G. Multiple optomechanically induced transparency in two-cavities optomechanical system via an optical parametric amplifier. *Eur. Phys. J. Plus* **2024**, *139*, 800. [CrossRef]
41. Li, W.A.; Huang, G.Y. Enhancement of optomechanically induced sum sidebands using parametric interactions. *Phys. Rev. A* **2019**, *100*, 023838. [CrossRef]
42. Wang, X.Y.; Si, L.G.; Lu, X.H.; Wu, Y. Generation and enhancement of sum sideband in a quadratically coupled optomechanical system with parametric interactions. *Opt. Express* **2019**, *27*, 29297–29308. [CrossRef]
43. Zhang, W.; Shen, H. Optomechanical second-order sidebands and group delays in a spinning resonator with a parametric amplifier and non-Markovian effects. *Phys. Rev. A* **2024**, *109*, 033701. [CrossRef]
44. Wang, B.; Liu, Z.X.; Kong, C.; Xiong, H.; Wu, Y. Mechanical exceptional-point-induced transparency and slow light. *Opt. Express* **2019**, *27*, 8069–8080. [CrossRef]
45. Massel, F.; Heikkilä, T.T.; Pirkkalainen, J.M.; Cho, S.U.; Saloniemi, H.; Hakonen, P.J.; Sillanpää, M.A. Microwave amplification with nanomechanical resonators. *Nature* **2011**, *480*, 351–354. [CrossRef]
46. Li, W.; Li, C.; Song, H. Theoretical realization and application of parity-time-symmetric oscillators in a quantum regime. *Phys. Rev. A* **2017**, *95*, 023827. [CrossRef]
47. Lü, X.Y.; Jing, H.; Ma, J.Y.; Wu, Y. PT-symmetry-breaking chaos in optomechanics. *Phys. Rev. Lett.* **2015**, *114*, 253601. [CrossRef]

Disclaimer/Publisher's Note: The statements, opinions and data contained in all publications are solely those of the individual author(s) and contributor(s) and not of MDPI and/or the editor(s). MDPI and/or the editor(s) disclaim responsibility for any injury to people or property resulting from any ideas, methods, instructions or products referred to in the content.